ACS OMEGA

Open Access

http://pubs.acs.org/journal/acsodf

Article

Repurposing Cotton Gin Trash for Cellulose Nanofibril−Silver Hybrid and Ultralight Silver-Infused Aerogel

Sunghyun Nam,* Michael W. Easson, Jacobs H. Jordan, Zhongqi He, Isabel M. Lima, Matthew B. Hillyer, Nicholas E. Ernst, David Fang, and Md Muhaiminul Islam

Cite This: *ACS Omega* 2024, 9, 38195−38204

Read Online

ACCESS | Metrics & More | Article Recommendations

ABSTRACT: Cellulose nanofibril−silver (CNF−Ag) hybrid and ultralight silver-infused aerogel were produced using cotton gin trash (CGT), an abundant agro-waste material. This repurposing of CGT was achieved by exploiting its potential for CNF extraction and the in situ synthesis of silver nanoparticles (Ag NPs). CNFs were extracted from CGT through a mechanical shearing process. These CNFs served as a multifunctional nanotemplate for the controlled reduction of Ag ions, efficient nucleation, and stabilization of NPs, resulting in the production of a high concentration of Ag NPs (ca. 19 wt %) within the CNFs. Transmission electron microscopy images of cross-sectioned CNFs confirmed the uniform dispersion of NPs (ca. 18 nm diameter) inside the CNFs. Rietveld refinement analysis of X-ray diffraction patterns revealed that CNFs produced smaller Ag crystallites compared to CGT microparticles. The CNF−Ag hybrid was then fabricated into an aerogel using freeze-drying, with its weight being light enough to rest on a cotton flower's stamen. The infusion of Ag NPs led to approximately 20% reductions in the specific surface area and pore volume of the aerogel.

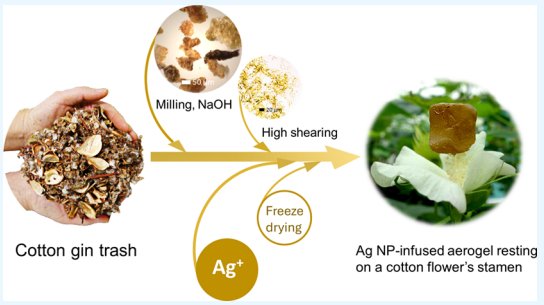

INTRODUCTION

Cotton gin trash (CGT) is a byproduct generated during the cotton ginning process, which separates cotton fibers from seed bolls. This waste material consists of a mixture of hulls, leaves, sticks, and motes, comprising cellulose, lignin, hemicellulose, and various inorganic components.[1,2] CGT primarily contains cellulose (approximately 30%), hemicellulose (10%), and lignin (19%),[1] along with trace amounts (20−130 ppm) of various inorganics.[2] The amount of CGT generated depends on factors such as harvesting methods, ginning techniques, and cotton variety, typically constituting 16−65% of the total weight per bale of cotton.[3] Considering 14.7 million bales of cotton were ginned in the United States per year between 2021 and 2023,[4] around 1.3×10^9 kg of CGT were produced annually. Current disposal methods for CGT include composting for soil amendment and livestock feed.[3,5] However, these approaches have limitations and the growing interest in the circular economy has led to a strong demand for novel ways to repurpose CGT for material applications.[6−8] Examples of CGT repurposing methods include films,[9,10] composites,[11,12] packaging,[13] particleboard,[14] adsorbent materials,[15] and nanocellulose.[1]

Cellulose nanofibrils (CNFs), fibers with widths of nanometer-scale and lengths up to several microns, have been prepared by liberating elementary fibrils from biomass materials containing fiber matrices and microfiber bundles.[16] These biomass sources include wood pulp, wheat straw, soy hull, and sugar cane bagasse, among others. However, relatively little attention has been given to utilizing CGT as a source material for CNFs. Only recently has CGT begun to be used for the preparation of cellulose nanocrystals.[1]

The production of CNFs generally involves the chemical extraction of celluloses, which requires purification to remove noncellulosic components such as hemicelluloses and lignin. Hemicellulose is a polysaccharide with an amorphous, branched structure, acting as a compatibilizer between cellulose and lignin.[17,18] Lignin, on the other hand, is a polyphenolic molecule with intricate aromatic ring structures and linkages that contributes to the stiffness of plant cell walls and hydrophobicity.[19] Various methods have been employed for defibrillation. For instance, cryocrushing and mechanical techniques were used for wheat straw and soy hull after bleaching and acid treatments.[20] Alternatively, wet-disk milling and ultrafine grinding were used to isolate CNFs from waste sludge.[21] A combination of ultrasound and enzymatic treatment extracted CNFs from curauá and bagasse fibers.[22]

Received: June 19, 2024
Revised: August 22, 2024
Accepted: August 26, 2024
Published: August 28, 2024

The exceptional physicochemical properties of NPs have led to the development of various synthetic methods for their production. However, most of these methods require reducing agents to convert Ag ions into Ag atoms and stabilizing agents to control particle size and shape during particle growth and prevent particle aggregation. The high cost and toxicity of these reducing and stabilizing agents often pose a barrier to the sustainable production of NPs.[23,24] For instance, common reducing agents such as hydrazine, sodium borohydride, and *N*,*N*-dimethylformamide are environmentally and biologically hazardous. The growing interest in "green chemistry" encourages the exploration of environmentally friendly alternatives with effective reducing and stabilizing properties.

In this study, we utilized CNFs from CGT as a "green" multifunctional nanotemplate. Instead of removing non-cellulosic components such as hemicellulose and lignin from CGT, we advantageously employed them as reducing agents. Our previous study demonstrated the remarkable reducing properties of galactose-containing vicinal diols in hemicellulose and aldehyde groups in lignin within CGT.[25] We examined the reducing properties of CGT in the form of CNFs, which are expected to enhance the accessibility of their reducing sites. CNFs are also anticipated to serve as an ideal host to stabilize and immobilize NPs, preventing their aggregation. The synthesis and formation of NPs within the CNF host were investigated. Using the obtained CNF−Ag hybrid, an ultralight aerogel was produced through freeze-drying. Due to their unique structural and functional characteristics including a high specific surface area, porous network, biodegradability, and biocompatibility, CNF aerogels have received significant attention in various fields such as pharmaceuticals,[26] packaging,[27] insulation,[28] and tissue engineering.[29] The incorporation of Ag NPs, known for their intrinsic antimicrobial properties, into CNF aerogels can enhance their functionality. These nanocomposite materials show promise in applications including biomedical fields, particularly in would treatment,[30] renewable catalysts for diverse chemical reactions,[31] and water purification.[32] This study explores the effects of incorporating Ag NPs on CNF aerogels, focusing on changes in morphology, specific surface area, and pore volume. This approach not only offers a sustainable and environmentally friendly method for synthesizing Ag NPs but also advances the development of functional aerogel materials using CGT.

EXPERIMENTAL SECTION

Materials. Cotton gin trash was obtained from the USDA Research Facility in Stoneville, Mississippi. Silver nitrate ($AgNO_3$, 99.9%) was purchased from J. T. Baker (Radnor, PA, USA). Sodium hydroxide (NaOH), methyl methacrylate, butyl methacrylate, methyl ethyl ketone, and benzoyl peroxide were purchased from Sigma-Aldrich (St. Louis, MO, USA). All chemicals were used as received without further purification. Deionized (DI) water was used as a solvent.

Fabrication of CNFs from CGT. CGT was ground in a Wiley mill (E3300, Eberbach Corp., Belleville, MI, USA) with a 60 mesh sieve. The obtained powder sample was treated for 2 h at 60 °C with a 4% (w/w) NaOH solution at a sample-to-liquor ratio of 1:20 (w/v) to remove extractives. The sample was subsequently washed with deionized water until a neutral eluant (pH ≈ 7) was achieved. The alkali-treated CGT was suspended in deionized water at approximately 0.5% (w/w) using an Ultra-Turrax (T25, IKA Works, Inc., Wilmington, NC, USA) mechanical homogenizer. The slurry was then subjected to high-shear mixing with a Silverson L5M-A Laboratory Mixer equipped with a Square Hole High Shear Screen at 8000 rpm for 10 min. The obtained cellulose slurry was further subjected to high-shearing forces using a high-pressure homogenizer (Microfluidizer M-110P, Microfluidics Corp., Newton, MA, USA). The suspension was pumped through one 200 μm ceramic interaction chamber five times, and then one 87 μm diamond Z-shaped interaction chamber was added in series with the 200 μm ceramic interaction chamber for an additional five passes. The operating pressure was set to 2100 MPa.

Fabrication of CNF−Ag Hybrid. A 10 mL aqueous solution of $AgNO_3$ (58 mM) was added to a 50 mL suspension of CNFs. The resulting solution was heated at 100 °C for 30 min. After treatment, the CNFs were rinsed with DI water (approximately 0.5% w/w) multiple times using a centrifuge (Eppendorf 5810, FA-45-6-30 rotor, 10,000 × *g*, 10 min).

Fabrication of Aerogel. A 5 mL aqueous suspension containing approximately 1% w/w of CNFs was poured into a 20 mL disposable borosilicate vial. The vial was then placed into a shallow vacuum Dewars containing liquid nitrogen and frozen for at least ten minutes. The frozen vial was removed from the Dewars and immediately placed into a vacuum-safe flask and lyophilized using a VirTis Freezemobile 25EL freeze-dryer (ATS, Warminster, PA USA) at 15 mT over 72 h.

Characterization. Photographs of samples were taken using a digital camera (RX100, Sony). Optical microscopic images of samples were obtained in reflection mode using a digital microscope (KH-8700, Hirox).

Ultraviolet−visible (UV−vis) spectra were collected using a UV−vis spectrometer (ISR-2600, Shimadzu) equipped with an integrating sphere unit. Absorbance spectra were collected in the wavelength range of 200−1100 nm.

Scanning electron microscopy (SEM), energy-dispersive X-ray spectroscopy (EDS), and elemental mapping analyses were conducted using a Phenom G6 ProX SEM equipped with an EDS detector (Nanoscience Instruments, Phoenix, AZ, USA). A sample was mounted on a stub using double-sided carbon tape, followed by sputtering a 5 nm-thick gold coating onto the sample using a LUXOR sputter coater (Aptco Technologies, Nazareth, Belgium). Accelerating voltages of 10 kV and 15 kV were used for SEM and EDS, respectively. Field emission SEM (FE SEM) images were taken using a FEI Quanta 3D FEG FIB/SEM. The field emission gun was operated at an accelerating voltage of 5 kV and a gun current of 3.0 pA. The sample was mounted on a stub using double-sided carbon tape, and a platinum coating was sputtered onto the sample.

Transmission electron microscopic (TEM) images were obtained using a TEM (JEM-2011, Jeol) operating at 200 kV. For the sample preparation, a sample was embedded into a mixture of methyl methacrylate, butyl methacrylate, and benzoyl peroxide, which was polymerized using a UV cross-linker (UVP CL-1000, Analytik Jena) for 30 min following published techniques.[33,34] A block of the polymerized sample was then cut into approximately 100 nm-thick slices using a microtome (PowerTome Ultramicrotome, Boeckeler Instruments). These thin films were placed on a carbon-film-coated copper grid. The size of Ag NPs was determined by analyzing TEM micrographs using Image-J software.[35]

X-ray diffraction (XRD) measurements were conducted using an Empyrean diffractometer (Malvern Panalytical, Malvern, United Kingdom) with Cu Kα-radiation (1.5418 Å). Data was collected with a spinning zero-background

https://doi.org/10.1021/acsomega.4c05728
ACS Omega 2024, 9, 38195−38204

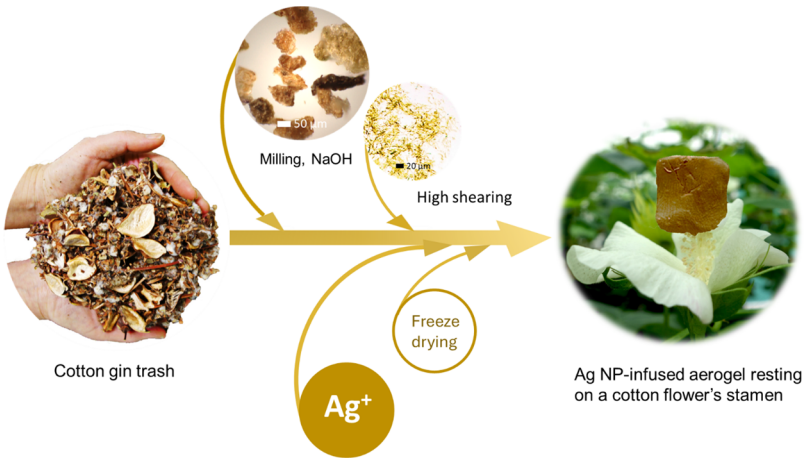

Figure 1. Schematic representation of the production of CNF−Ag hybrid and Ag-infused aerogel derived from cotton gin trash (CGT).

sample holder over the range of 5−80° 2θ, with a 0.013 step size and a radial divergence slit and nickel filter. A blank run of the sample holder was acquired prior to sample acquisition to capture the instrument background. The obtained powder patterns were analyzed using a pseudo-Voigt peak shape with the MAUD Rietveld program (Materials Analysis Using Diffraction, v. 2.93).[36,37] The cellulose Iβ crystal information file (.cif) was supplied by Nishiyama et al.[38,39] A cellulose II pattern with a crystallite size of 12 Å was used to model the amorphous phase.[40,41] The crystalline phases for silver ICSD 604629 were modeled with its crystal information file.[42] The relative percentage of each phase was determined based on the area of the refined powder patterns after background subtraction, relative to the area of the total calculated pattern for each refinement. The crystallinity of the sample was calculated by taking the area of the refined cellulose Iβ pattern representing crystalline cellulose divided by the sum of the area for the crystalline and amorphous regions. The cellulose crystallite size perpendicular to the (hkl) lattice plane (L_{hkl}) was calculated using the Scherrer equation[43,44]:

$$L_{hkl} = \frac{0.9\lambda}{\beta_{hkl} \times \cos\theta} \quad (1)$$

where the shape factor was taken as $K = 0.9$, λ is the average Cu Kα-radiation wavelength (1.5418 Å), β is the angular full-width half-maximum intensity (fwhm) in radians of the refined pattern, and θ is the scattering angle. The associated d-spacings were calculated from the refined unit cell dimensions. The Mercury 3.0 program[45] was used to calculate diffraction patterns and model crystallites. The crystallinity index (CI) was measured using the Segal method[46]:

$$\mathrm{CI}(\%) = \frac{I_t - I_a}{I_t} \times 100 \quad (2)$$

where I_t is the total intensity of the (200) peak at 22.7° 2θ, and I_a is the amorphous intensity at 18° 2θ.

The silver content was measured using a graphite furnace atomic absorption spectrometer (240Z AA, Agilent, Santa Clara, CA, USA). Approximately 0.05 g of CNFs was treated with 10 mL of 6 M nitric acid (Trace Metal grade) and digested in a microwave digestion system (MARS 6, CEM Corporation, Matthews, NC, USA). The digest was diluted by weight 1:1000 and analyzed with an external calibration curve, which was obtained using silver single-element standard (Agilent, Santa Clara, CA, USA). The average of three measurements was presented.

The specific surface area and pore size of aerogel samples were measured using a Quantachrome NOVA 2200e adsorption system (Quantachrome Instruments, Boynton Beach, FL). Samples were outgassed at 150 °C for 7 days under vacuum. Adsorption data were collected using 25 points on the nitrogen isotherm between 0.0499 and 0.9871 relative pressures at 77 K (−196 °C) and desorption data were collected using 12 points down to 0.04735 relative pressure at 77 K (−196 °C) (liquid nitrogen). The average of three measurements was presented.

RESULTS AND DISCUSSION

The objective of this study is to produce CNF−Ag hybrid and ultralight aerogel infused with Ag NPs using CGT, a byproduct of the cotton ginning process. Figure 1 shows the stepwise fabrication process from CGT byproduct to Ag NP-infused CGT aerogel. As can be observed from its photograph, CGT is a heterogeneous mixture of components, including burs, bracts, sticks, seeds, leaf fragments, and motes. The composition of CGT varies based on the harvesting method,[47,48] with differences in size, shape, and color among the components. According to a previous study,[1] the CGT studied in this study contains extractable (19.0%), celluloses (30.9%), hemicelluloses (9.7%), arabinan (1.5%), galactan (2.4%), acetate (2.8%), acid-soluble lignin (0.8%), acid-insoluble lignin (19.3%), ash (0.5%), and other (13.1%). The CGT was first homogenized by mechanical milling into powder with particle sizes smaller than 250 μm. The powder then underwent alkali treatment to remove water-soluble extractable materials, including inorganic salts, nonstructural sugars, nitrogenous material, soil particulates, fertilizers, waxes, and other minor components, which complicate subsequent workup and characterization steps.[1,49,50] Subsequently, the treated powder was transformed into CNFs using a high-shearing process. The CNFs were heated in an aqueous solution containing Ag ions, initiating the in situ synthesis of Ag NPs. Finally, freeze-drying the aqueous CNF suspension resulted in the production of an ultralight Ag-infused aerogel. The aerogel's ultralight nature, with an apparent density of 0.01 g/cm^3, was demonstrated by its ability to rest on the stamens of a cotton flower. Its specific surface area and pore volume were 9.2 and 30 mm^3/g, respectively.

https://doi.org/10.1021/acsomega.4c05728
ACS Omega 2024, 9, 38195−38204

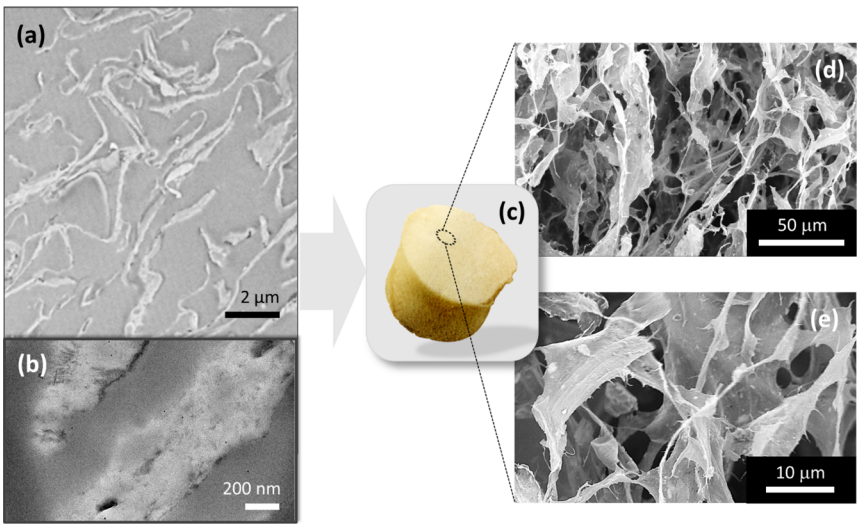

Figure 2. TEM images of CNFs from CGT at (a) low and (b) high magnifications. (c) Photograph of an aerogel fabricated from CNFs and its SEM images at (d) low and (e) high magnifications.

Figure 2 shows the morphological characteristics of the CGT-derived CNFs and the resulting aerogel. The TEM images of the CNFs at low and high magnifications (Figure 2a,b, respectively) reveal that the thickness of CNFs ranged from 100 to 500 nm, with lengths extending up to several microns. The CNFs exhibited a yellow color due to the presence of phenolic-based constituents like lignin, which remained after the alkaline treatment. Consequently, the aerogel fabricated from these CNFs also displayed a yellow hue (Figure 2c). SEM images of the aerogel at varying magnifications demonstrate that the fibrillated fibers were uniformly distributed without agglomeration (Figure 2d,e). The aerogel exhibited a highly porous network structure with numerous gaps.

To create a CNF−Ag hybrid, we exploited the ability of CNFs to transform Ag ions into Ag NPs. Previous studies have demonstrated that CGT powder[25] and raw cotton fiber varieties[51−54] could synthesize Ag NPs in situ by acting as reducing and stabilizing agents. A simple heat treatment with an Ag precursor initiated this self-synthesis process. The noncellulosic components in CGT, such as hemicellulose and lignin, possess remarkable reducing properties.[25] Galactose-containing vicinal diols of hemicellulose reduce Ag ions to Ag atoms through oxidation to a dialdehyde product. The aldehyde groups in lignin reduce Ag ions via hydration to a geminal diol followed by oxidation to carboxylic acids. The direct reduction of Ag ions at the reducing sites in CGT allows for nucleation, nuclei growth, and particle growth in CGT, resulting in the in situ formation of NPs. Consequently, additional chemical agents like reducing and stabilizing agents, typically required in conventional synthetic methods of NPs, are unnecessary for this natural synthesis process. Figure 3 shows the optical properties of CNFs before and after the in situ synthesis of Ag NPs. Optical microscopy images display the yellow coloration of CNFs following their self-synthesis, attributed to the surface plasmon resonance of NPs (Figure 3a,b). UV−vis spectroscopy further confirms the presence of a surface plasmon resonance peak (Figure 3c). CGT microparticles (no alkaline treatment) exhibited higher absorbance at lower wavelengths, which diminished upon conversion into CNFs. These unique spectra suggest that certain polyphenolic

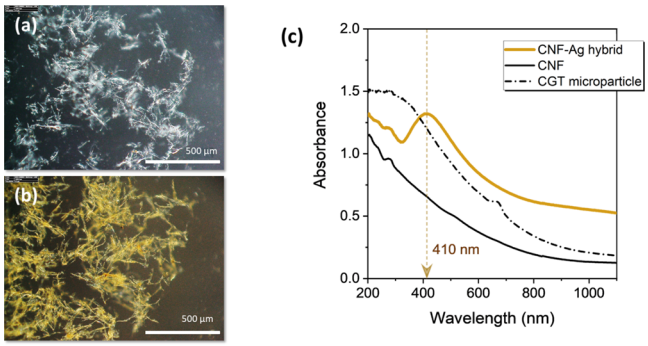

Figure 3. Optical microscopic images of CGT (a) before and (b) after in situ synthesis of Ag NPs. (c) UV−vis spectra of CNF−Ag hybrid, CNF, and CGT microparticle.

substances like tannins, which absorb in the ultraviolet region (255−330 nm), were extracted during the CNF fabrication process, i.e., alkaline treatment. Additionally, the small size of the CNFs contributed to the reduced absorbance. After treatment, CNFs exhibited a new peak centered at 410 nm, corresponding to the surface plasmon resonance absorbance of Ag NPs. The emergence of a strong, well-defined peak indicates the formation of abundant Ag NPs by CNFs. The Ag NP content was determined to be 18.9 ± 3.5% based on the dry weight of CNFs.

The formation of Ag NPs on the exterior and interior of CNFs was analyzed using FE-SEM and TEM, respectively. The FE-SEM image (Figure 4a) reveals sphere-like Ag NPs, approximately 20 nm in diameter, formed on the surface of the CNFs. TEM images of cross-sectioned CNFs at low magnifications (Figure 4b−e) show a varying density of NPs between CNFs. Some CNFs produced more NPs than others (Figure 4b,e), and the population of NPs was also nonuniform within individual CNFs (Figure 4c). This heterogeneity in NP formation can be attributed to the diverse composition of CGT. For example, CNFs derived from burs or sticks could generate more NPs than those from motes due to their higher lignin content. High-magnification TEM images of the CNF−Ag hybrid demonstrate the dispersion of individual NPs throughout the CNFs without aggregation (Figure 5a−e).

https://doi.org/10.1021/acsomega.4c05728
ACS Omega 2024, 9, 38195−38204

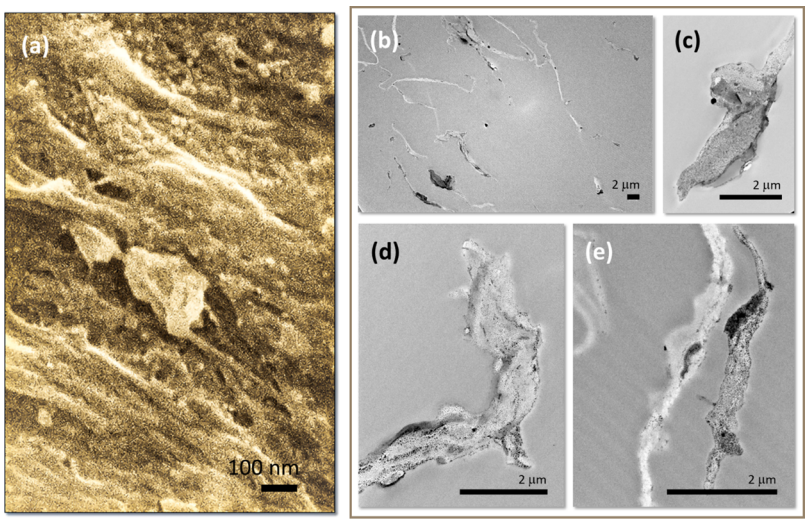

Figure 4. (a) FE SEM image of the surface of CNF−Ag hybrid and (b−e) TEM images of cross-sectioned CNF−Ag hybrid at low magnifications.

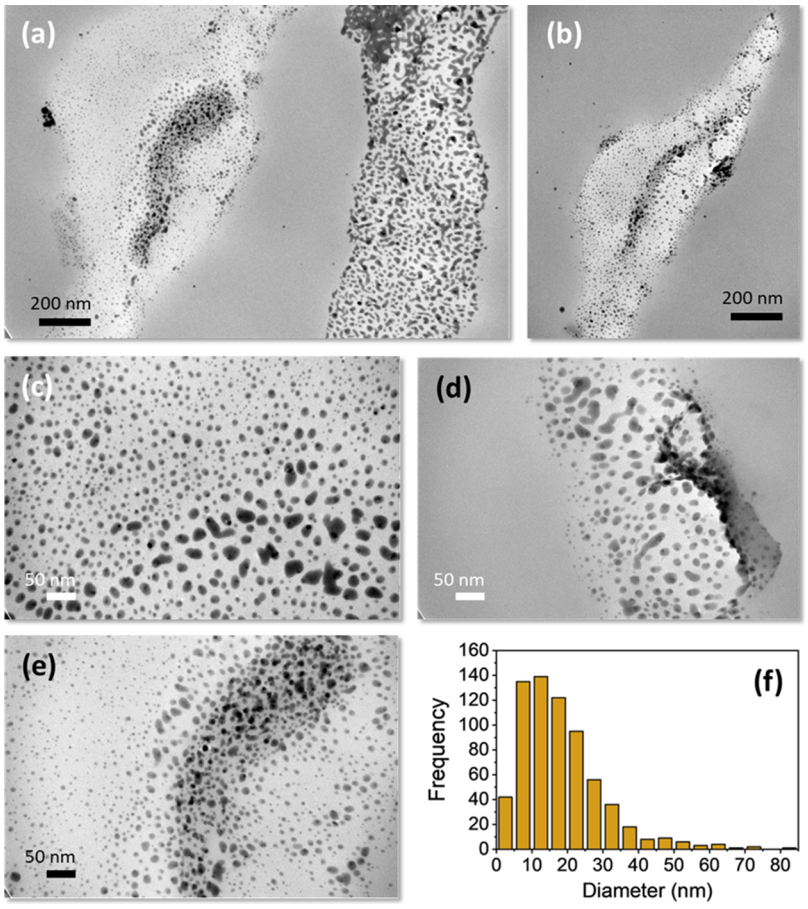

Figure 5. (a−e) TEM images of cross-sectioned CNF−Ag hybrid at high magnifications and (f) the size distribution histogram of Ag NPs formed within CNFs.

These internal NPs share a sphere-like morphology with those found on the CNF surface. Figure 5f presents a histogram of particle diameters measured from TEM micrographs, revealing a positively skewed (right-skewed) size distribution with a higher population of smaller-sized NPs. The average diameter was determined to be 18.2 ± 7.3 nm.

Figure 6 presents XRD patterns for CNF and CNF−Ag hybrid alongside the published XRD pattern of CGT.[25] Like CGT microparticles, CNF exhibited peaks corresponding to cellulose Iβ lattice planes: 14.8° 2θ, 16.6° 2θ, 22.4° 2θ, and 34.4° 2θ. These peaks appeared slightly better defined because of the loss of some amorphous materials including alkali-soluble extractives and hemicellulose during CNF fabrication.[50] Small peaks from salt impurities[50] were observed for both CGT microparticles and CNFs. Notably, the impurity peak at 26.6° 2θ intensified, and a new small impurity peak

https://doi.org/10.1021/acsomega.4c05728
ACS Omega 2024, 9, 38195−38204

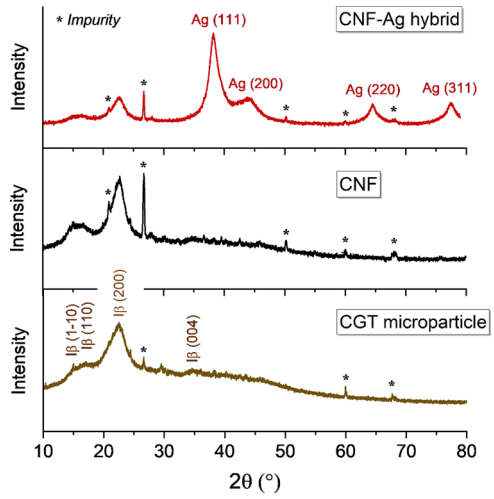

Figure 6. XRD patterns of CNF−Ag hybrid, CGT CNF, and CGT microparticle. The lattice planes of cellulose Iβ and Ag are labeled. An asterisk (*) denotes an impurity present in CGT.

emerged at 50.1° 2θ for CNF. These changes indicate that the alkaline treatment during CNF production led to the crystallization of certain impurities. The formation of Ag NPs by CNFs was confirmed by their XRD pattern. Four strong peaks at 38.1° 2θ, 44.0° 2θ, 64.4° 2θ, and 77.4° 2θ were attributed to the (111), (200), (220), and (311) lattice planes of a cubic silver crystal, respectively. In contrast to a previous study[25] that reported the detection of additional silver oxide peaks for CGT particles, no such corresponding peaks were observed in the XRD pattern for CNFs in this investigation. This result suggests a difference in the formation or stability of Ag species within the CNF structure compared to the CGT microparticles. The absence of silver oxide peaks indicates a potentially more controlled reduction process in the CNFs, leading to the exclusive formation of Ag NPs without significant oxidation. This finding highlights the potential advantages of utilizing CNFs for the synthesis of Ag NPs, as it offers a more efficient and precise method for obtaining pure Ag NPs without the presence of undesired oxide products.

To study the characteristics of crystallites within the CNF−Ag hybrid, a Rietveld refinement analysis was performed on its experimental XRD pattern. This analysis incorporated various parameters, such as scale factor, background function, crystallite sizes, crystallite dimensions, March-Dollase preferred orientation, and volume fractions of phases. The calculated XRD pattern of the CNF−Ag hybrid, along with those of multiple phases—cellulose Iβ, amorphous cellulose, background, and Ag—were obtained. The Rietveld refinement resulted in a satisfactory fit between the experimental and calculated results, with a weighted residual of least-squares refinement of 3.78. Figure 7a presents the refinement results for cellulose, indicating that CNFs were partially crystalline, comprising a mixture of crystalline cellulose (cellulose Iβ) and amorphous cellulose. The asymmetric unit cell of cellulose Iβ derived from its crystal information file shows two cellulose molecules positioned in parallel (Figure 7b). Table 1 compares

Table 1. Cellulose Parameters Determined from the Rietveld Refinement Analysis and CI Values Measured from the Segal Method for CGT Microparticle, CGT CNF, and CNF−Ag Hybrid

parameter		CGT microparticle[25]	CGT CNF	CNF−Ag hybrid
cellulose Iβ unit cell dimension (Å)	*a*	7.98	7.87	7.86
	b	8.19	8.61	8.11
	c	10.56	10.19	10.65
	γ	94.89	95.22	94.24
crystallite size (Å)	(200)	36.7	46.8	57.9
	(1−10)	34.7	53.8	59.1
	(110)	38.1	41.9	56.9
crystallinity (%)		32.3	35.3	34.9
CI (%)		37.6	47.6	39.2

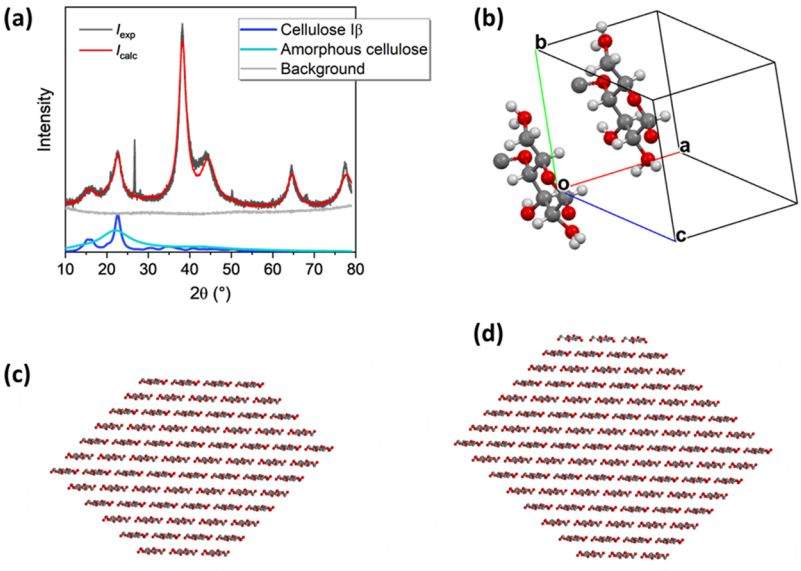

Figure 7. (a) Experimental and calculated XRD patterns of CNF−Ag hybrid obtained by Rietveld refinement including cellulose Iβ, amorphous cellulose, and background components. (b) Cellulose Iβ unit cell obtained from its crystal information file. Models of cellulose Iβ crystallite for (c) CNF and (d) CNF−Ag hybrid by diagonal truncation based on the dimensions along the (200), (1−10), and (110) lattice planes.

https://doi.org/10.1021/acsomega.4c05728
ACS Omega 2024, 9, 38195−38204

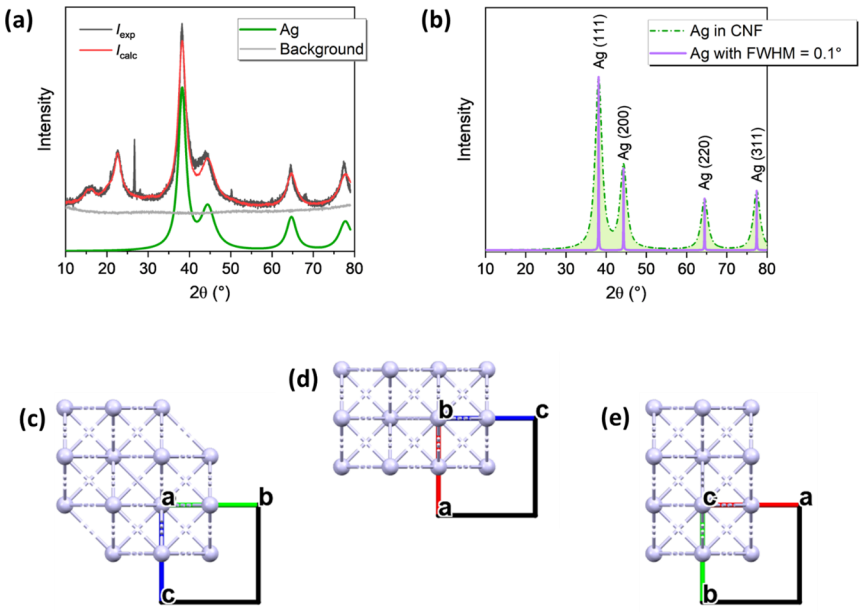

Figure 8. (a) Experimental and calculated XRD patterns of CNF−Ag hybrid obtained by Rietveld refinement, including Ag and background components. (b) Calculated XRD pattern of the Ag crystallite formed by CNF plotted with that of a perfect Ag crystallite with a 0.1 degree fwhm. (c−e) Views of the Ag unit cell derived from its crystal information file from different axes.

the cellulose Iβ unit cell dimensions, cellulose Iβ crystallite size, crystallinity, and CIs for CGT microparticles, CNF, and CNF−Ag hybrid. The cellulose Iβ unit cell dimensions remained consistent after CNF fabrication and Ag NP synthesis. However, the CNF fabrication process increased the crystallite sizes of cellulose Iβ along the (200) (1−10) and (110) orientations, with both CNF fabrication and Ag NP synthesis procedures further increasing them by about 60%. Crystallite models for cellulose Iβ before (Figure 7c) and after (Figure 7d) in situ synthesis of Ag NPs were constructed using calculated *d*-spacings and diagonal truncation, which terminates along the (200), (1−10), and (110) lattice planes. The CNF fabrication increased the proportion of the crystalline phase, while subsequent Ag NP synthesis slightly lowered the crystallinity. CNF−Ag hybrid contained around 35% crystalline cellulose (65% amorphous cellulose). The CI values measured using the Segal method were slightly greater than the crystallinity values determined from the Rietveld refinement analysis for all samples. However, both methods agreed on the effects of CNF fabrication and Ag NP incorporation on the proportion of the crystalline phase.

Figure 8a shows the Ag phase from the Rietveld refinement analysis. A diffraction pattern of a completely periodic Ag crystallite was constructed from its unit cell (Figure 8b), with fwhm set to 0.1 degrees and CuKα wavelength at 1.54056 Å. Unit cell views from the *a*, *b*, and *c* axes are presented in Figure 8c−e, respectively. Compared to its perfect crystal pattern, the diffraction peaks of Ag in CNF were considerably broader, suggesting the formation of small crystallites. The Ag crystallite size in CNF was determined from the Rietveld refinement analysis and compared with Ag in CGT microparticles[25] (Table 2). The analysis revealed that the Ag crystallites produced by CNF were smaller in size compared to those generated by CGT microparticles across all lattice planes. This finding suggests that the CNF structure influences the formation of smaller Ag crystallites. The determined *d*-spacing of Ag in CNFs was found to be similar to that of Ag in CGT microparticles.

Table 2. Crystallite Sizes and *d*-Spacings for Lattice Planes Determined from the Rietveld Refinement Analysis for Ag Formed in CGT Microparticle and CGT CNF

			crystallite size (Å)		*d*-spacing (Å)	
h	*k*	*l*	CGT microparticles[25]	CGT CNF	CGT microparticles[25]	CGT CNF
1	1	1	79.3	49.5	2.360	2.351
2	0	0	43.0	28.1	2.044	2.036
2	2	0	70.2	44.1	1.445	1.440
3	1	1	60.1	38.2	1.232	1.228

An aerogel was fabricated from the CNF−Ag hybrid using a freeze-drying process, which is considered more economical and efficient than other drying methods.[55] Figure 9a shows a photograph of the aerogel. Optical microscopic and SEM images of the CNF−Ag hybrid and Ag-infused CGT aerogel are presented in Figure 9b,c, respectively. The Ag-infused CGT aerogel exhibited a porous network structure similar to that of the CGT aerogel (Figure 2e). The obtained cylindrical Ag-infused aerogel with a volume of approximately 3.5 cm^3 could stand on a cotton flower stamen without causing its bending (Figure 1), indicating an ultralight attribute of the product. The apparent density of the aerogel was 0.01 g/cm^3. The specific surface area and pore volume of the Ag-infused CGT aerogel were 9.2 m^2/g and 30 mm^3/g, respectively, which were found to be approximately 20% smaller than those of the CGT aerogel (Figure 9d,e, respectively).

CONCLUSIONS

This study has demonstrated the potential of CGT as a sustainable and multifunctional material with diverse applications including the production of CNFs and functional ultralight aerogels. The high shearing process employed in the study proved effective in fabricating CNFs, which served as a versatile nanotemplate for Ag NP synthesis. By functioning as

https://doi.org/10.1021/acsomega.4c05728
ACS Omega 2024, 9, 38195−38204

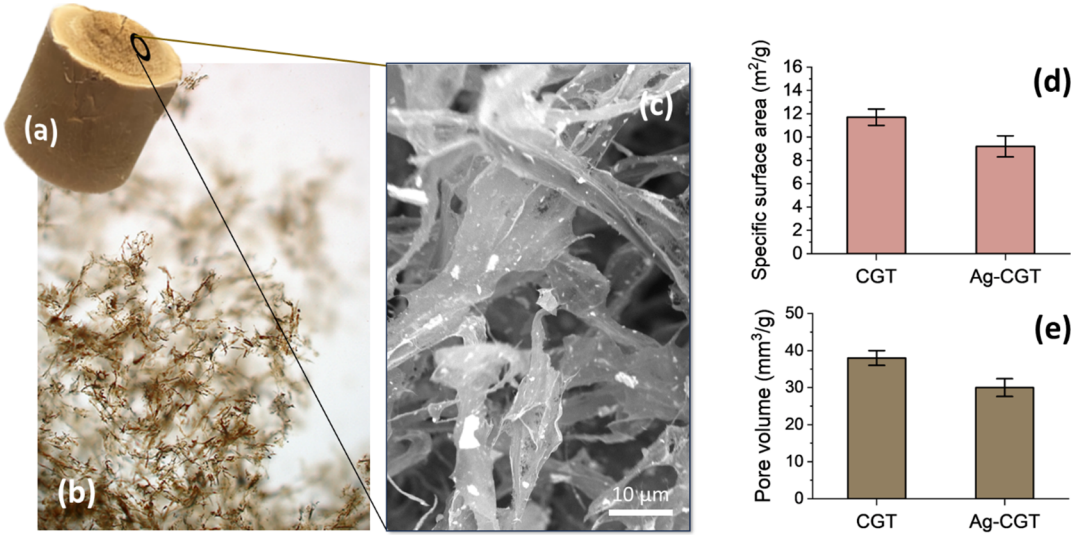

Figure 9. (a) Photograph of the aerogel fabricated from CNF−Ag hybrid. (b) Optical microscopic image of CNF−Ag hybrid and (c) SEM image of the Ag-infused CGT aerogel. (d) Specific surface areas and (e) pore volumes of the CGT aerogel and Ag-infused CGT aerogel.

a nucleation site, reducing agent, and stabilizing agent, the CNFs facilitated the production of a high concentration of Ag NPs both on the surface and within the CNFs. The formation of Ag NPs was confirmed through the observation of surface plasmon resonance of the resulting CNF−Ag hybrid. TEM images further validated the internal NP formation, revealing uniformly dispersed Ag NPs throughout the entire volume of the CNFs. The Rietveld refinement analysis of XRD patterns provided insights into the cellulose crystalline structure and the characteristics of Ag NPs. It was observed that the fabrication of CNFs and the in situ synthesis of Ag NPs led to an increase in the crystallite size of cellulose Iβ in CGT without significantly affecting its crystallinity. Moreover, the crystallite size of Ag NPs produced by CGT CNF was found to be slightly smaller than that produced by CGT microparticles. An aerogel fabricated from the CGT nanofiber−Ag hybrid exhibited ultralight characteristics. The infusion of Ag NPs into aerogel is expected to provide antimicrobial properties, and its performance will be the focus of future studies.

AUTHOR INFORMATION

Corresponding Author

Sunghyun Nam − *Cotton Fiber Bioscience and Utilization Research Unit, U.S. Department of Agriculture, Agricultural Research Service, Southern Regional Research Center, New Orleans, Louisiana 70124, United States;* orcid.org/0000-0002-4059-606X; Phone: +1 504 286 4229; Email: sunghyun.nam@usda.gov

Authors

Michael W. Easson − *Cotton Quality and Innovation Research Unit, U.S. Department of Agriculture, Agricultural Research Service, Southern Regional Research Center, New Orleans, Louisiana 70124, United States;* orcid.org/0000-0002-2268-1922

Jacobs H. Jordan − *Commodity Utilization Research Unit, U.S. Department of Agriculture, Agricultural Research Service, Southern Regional Research Center, New Orleans, Louisiana 70124, United States;* orcid.org/0000-0002-0238-3864

Zhongqi He − *Commodity Utilization Research Unit, U.S. Department of Agriculture, Agricultural Research Service, Southern Regional Research Center, New Orleans, Louisiana 70124, United States*

Isabel M. Lima − *Commodity Utilization Research Unit, U.S. Department of Agriculture, Agricultural Research Service, Southern Regional Research Center, New Orleans, Louisiana 70124, United States*

Matthew B. Hillyer − *Cotton Fiber Bioscience and Utilization Research Unit, U.S. Department of Agriculture, Agricultural Research Service, Southern Regional Research Center, New Orleans, Louisiana 70124, United States;* orcid.org/0000-0002-3960-7657

Nicholas E. Ernst − *Department of Chemistry, Purdue University Northwest, Hammond, Indiana 46323, United States*

David Fang − *Cotton Fiber Bioscience and Utilization Research Unit, U.S. Department of Agriculture, Agricultural Research Service, Southern Regional Research Center, New Orleans, Louisiana 70124, United States*

Md Muhaiminul Islam − *Department of Chemistry, Tulane University, New Orleans, Louisiana 70118, United States;* orcid.org/0009-0007-0285-8632

Complete contact information is available at: https://pubs.acs.org/10.1021/acsomega.4c05728

Notes

The authors declare no competing financial interest.

ACKNOWLEDGMENTS

This research was supported by the ARS Innovation Fund. The authors would like to thank the LSU Shared Instrument Facility for their assistance in data collection. This research was supported by the U.S. Department of Agriculture, Agricultural Research Service. Mention of trade names or commercial products is solely for the purpose of providing specific information and does not imply recommendation or endorsement by USDA. USDA is an equal opportunity provider and employer.

https://doi.org/10.1021/acsomega.4c05728
ACS Omega 2024, 9, 38195−38204

REFERENCES

(1) Jordan, J. H.; Easson, M. W.; Dien, B.; Thompson, S.; Condon, B. D. Extraction and characterization of nanocellulose crystals from cotton gin motes and cotton gin waste. *Cellulose* **2019**, *26*, 5959−5979.

(2) Zabaniotou, A.; Andreou, K. Development of alternative energy sources for GHG emissions reduction in the textile industry by energy recovery from cotton ginning waste. *J. Clean. Prod.* **2010**, *18*, 784−790.

(3) Thomasson, J. A. A review of cotton gin trash disposal and utilization. In *Beltwide cotton conferences*; 1990; pp 689−705.

(4) Shahbandeh, M. *U.S. cotton production 2001−2021*; 2022. https://www.statista.com/statistics/191500/cotton-production-in-the-us-since-2000/.

(5) Stewart, L. *Using cotton byproducts in beef cattle diets*; University of Georgia, 2010.

(6) McIntosh, S.; Vancov, T.; Palmer, J.; Morris, S. Ethanol production from cotton gin trash using optimized dilute acid pretreatment and whole slurry fermentation processes. *Bioresour. Technol.* **2014**, *173*, 42−51.

(7) Agblevor, F. A.; Cundiff, J. S.; Mingle, C.; Li, W. Storage and characterization of cotton gin waste for ethanol production. *Resour. Conserv. Recycl.* **2006**, *46*, 198−216.

(8) Hamawand, I.; Sandell, G.; Pittaway, P.; Chakrabarty, S.; Yusaf, T.; Chen, G.; Seneweera, S.; Al-Lwayzy, S.; Bennett, J.; Hopf, J. Bioenergy from cotton industry wastes: a review and potential. *Renew. Sustain. Energy Rev.* **2016**, *66*, 435−448.

(9) Haque, A. N. M. A.; Remadevi, R.; Wang, X.; Naebe, M. Physicochemical properties of film fabricated from cotton gin trash. *Mater. Chem. Phys.* **2020**, *239*, No. 122009.

(10) Haque, A. N. M. A.; Remadevi, R.; Wang, X.; Naebe, M. Mechanically milled powder from cotton gin trash for diverse applications. *Powder Technol.* **2020**, *361*, 679−686.

(11) Ge, C.; Cheng, H. N.; Miri, M. J.; Hailstone, R. K.; Francis, J. B.; Demyttenaere, S. M.; Alharbi, N. A. Preparation and evaluation of composites containing polypropylene and cotton gin trash. *J. Appl. Polym. Sci.* **2020**, *137*, 49151.

(12) Bajwa, S. G.; Bajwa, D. S.; Holt, G.; Coffelt, T.; Nakayama, F. Properties of thermoplastic composites with cotton and guayule biomass residues as fiber fillers. *Ind. Crop. Prod.* **2011**, *33*, 747−755.

(13) Haque, A. N. M. A.; Naebe, M. Flexible water-resistant semi-transparent cotton gin trash/poly (vinyl alcohol) bio-plastic for packaging application: Effect of plasticisers on physicochemical properties. *J. Clean. Prod.* **2021**, *303*, No. 126983.

(14) Holt, G. A.; Chow, P.; Wanjura, J. D.; Pelletier, M. G.; Coffelt, T. A.; Nakayama, F. S. Termite resistance of biobased composition boards made from cotton byproducts and guayule bagasse. *Ind. Crop. Prod.* **2012**, *36*, 508−512.

(15) Haque, A. N. M. A.; Remadevi, R.; Rojas, O. J.; Wang, X.; Naebe, M. Kinetics and equilibrium adsorption of methylene blue onto cotton gin trash bioadsorbents. *Cellulose* **2020**, *27*, 6485−6504.

(16) Salas, C.; Nypelo, T.; Rodriguez-Abreu, C.; Carrillo, C.; Rojas, O. J. Nanocellulose properties and applications in colloids and interfaces. *Curr. Opin. Colloid Interface Sci.* **2014**, *19* (5), 383−396.

(17) Chaker, A.; Alila, S.; Mutjé, P.; Vilar, M. R.; Boufi, S. Key role of the hemicellulose content and the cell morphology on the nanofibrillation effectiveness of cellulose pulps. *Cellulose* **2013**, *20* (6), 2863−2875.

(18) Pennells, J.; Godwin, I. D.; Amiralian, N.; Martin, D. J. Trends in the production of cellulose nanofibers from non-wood sources. *Cellulose* **2020**, *27* (2), 575−593.

(19) Gupta, A.; Simmons, W.; Schueneman, G. T.; Hylton, D.; Mintz, E. A. Rheological and Thermo-Mechanical Properties of Poly(lactic acid)/Lignin-Coated Cellulose Nanocrystal Composites. *ACS Sustain. Chem. & Eng.* **2017**, *5* (2), 1711−1720.

(20) Alemdar, A.; Sain, M. Isolation and characterization of nanofibers from agricultural residues: wheat straw and soy hulls. *Bioresour. Technol.* **2008**, *99* (6), 1664−1671.

(21) Jonoobi, M.; Mathew, A. P.; Oksman, K. Producing low-cost cellulose nanofiber from sludge as new source of raw materials *Ind. Crops Prod.* **2012**, *40*, 232−238.

(22) de Campos, A.; Correa, A. C.; Cannella, D.; Teixeira, M. E.; Marconcini, J. M.; Dufresne, A.; Mattoso, L. H. C.; Cassland, P.; Sanadi, A. R. Obtaining nanofibers from curauá and sugarcane bagasse fibers using enzymatic hydrolysis followed by sonication. *Cellulose* **2013**, *20* (3), 1491−1500.

(23) El-Seedi, H. R.; El-Shabasy, R. M.; Khalifa, S. A. M.; Saeed, A.; Shah, A.; Shah, R.; Iftikhar, F. J.; Abdel-Daim, M. M.; Omri, A.; Hajrahand, N. H.; et al. Metal nanoparticles fabricated by green chemistry using natural extracts: biosynthesis, mechanisms, and applications. *RSC Adv.* **2019**, *9*, 24539−24559.

(24) Palomo, J. M.; Filice, M. Biosynthesis of Metal Nanoparticles: Novel Efficient Heterogeneous Nanocatalysts. *Nanomaterials* **2016**, *6*, 84.

(25) Nam, S.; Easson, M.; Jordan, J. H.; He, Z.; Zhang, H.; Santiago Cintron, M.; Chang, S. Unveiling the hidden value of cotton gin waste: natural synthesis and hosting of silver nanoparticles. *ACS Omega* **2023**, *8*, 31281−31292.

(26) García-González, C. A.; Sosnik, A.; Kalmár, J.; De Marco, I.; Erkey, C.; Concheiro, A.; Alvarez-Lorenzo, C. Aerogels in drug delivery: From design to application. *J. Controlled Release* **2021**, *332*, 40−63.

(27) Mikkonen, K. S.; Parikka, K.; Ghafar, A.; Tenkanen, M. Prospects of polysaccharide aerogels as modern advanced food materials. *Trends Food Sci. Technol.* **2013**, *34*, 124−136.

(28) Demilecamps, A.; Beauger, C.; Hildenbrand, C.; Rigacci, A.; Budtova, T. Cellulose-silica aerogels. *Carbohydr. Polym.* **2015**, *122*, 293−300.

(29) Ghafari, R.; Jonoobi, M.; Amirabad, L. M.; Oksman, K.; Taheri, A. R. Fabrication and characterization of novel bilayer scaffold from nanocellulose based aerogel for skin tissue engineering applications. *Int. J. Biol. Macromol.* **2019**, *136*, 796−803.

(30) Wu, J.; Zheng, Y.; Wen, X.; Lin, Q.; Chen, X.; Wu, Z. Silver nanoparticle/bacterial cellulose gel membranes for antibacterial wound dressing: Investigation in vitro and in vivo. *Biomed. Mater.* **2014**, *9*, No. 035005.

(31) Arantes, A. C. C.; das Graças Almeida, C.; Dauzacker, L. C. L.; Bianchi, M. L.; Wood, D. F.; Williams, T. G.; Orts, W. J.; Tonoli, G. H. D. Renewable hybrid nanocatalyst from magnetite and cellulose for treatment of textile effluents. *Carbohydr. Polym.* **2017**, *163*, 101−107.

(32) Gia-Thien Ho, T.; Thao Truong, D. P.; Nguyen, H. B.; Long Do, B.; Dinh, T. A.; Ton-That, P.; Van Nguyen, T. T.; Ta Truong, T. B.; Ha Huynh, K. P.; Tri, T. Green synthesized nano-silver/cellulose aerogel as a robust active and recyclable catalyst towards nitrophenol hydrogenation. *J. Chem. Eng.* **2023**, *471*, No. 144604.

(33) Thibodeaux, D. P.; Evans, J. P. Cotton fiber maturity by image analysis. *Text. Res. J.* **1986**, *56*, 130−139.

(34) Boylston, E. K.; Hinojosa, O.; Hebert, J. J. A quick embedding method for light and electron microscopy of textile fibers. *Biotech. Histochem.* **1991**, *66* (3), 122−124.

(35) Schneider, C. A.; Rasband, W. S.; Eliceiri, K. W. NIH Image to ImageJ: 25 years of image analysis. *Nat. Methods* **2012**, *9*, 671−675.

(36) Foster, E. J.; Moon, R. J.; Agarwal, U. P.; Bortner, M. J.; Bras, J.; Camarero-Espinosa, S.; Chan, K. J.; Clift, M. J. D.; Cranston, E. D.; Eichhorn, S. J.; et al. Current characterization methods for cellulose nanomaterials. *Chem. Soc. Rev.* **2018**, *47*, 2609−2679.

(37) Mackin, R. T.; Fontenot, K. R.; Edwards, J. V.; Prevost, N. T.; Jordan, J. H.; Easson, M. W.; Condon, B. D.; French, A. D. Detection of human neutrophil elastase by fluorescent peptide sensors conjugated to TEMPO-oxidized nanofibrillated cellulose. *Int. J. Mol. Sci.* **2022**, *23* (6), 3101.

(38) Nishiyama, Y.; Langan, P.; Chanzy, H. Crystal structure and hydrogen-bonding system in cellulose Iβ from synchrotron X-ray and neutron fiber diffraction. *J. Am. Chem. Soc.* **2002**, *124*, 9074−9082.

(39) French, A. D. Idealized powder diffraction patterns for cellulose polymorphs. *Cellulose* **2014**, *21*, 885−896.

https://doi.org/10.1021/acsomega.4c05728
ACS Omega 2024, 9, 38195−38204

(40) Nam, S.; French, A. D.; Condon, B. D.; Concha, M. Segal crystallinity index revisited by the simulation of X-ray diffraction patterns of cotton cellulose Iβ and cellulose II. *Carbohydr. Poly.* **2016**, *135*, 1−9.
(41) Ling, Z.; Xu, F.; Edwards, J. V.; Prevost, N. T.; Nam, S.; Condon, B. D.; French, A. D. Nanocellulose as a colorimetric biosensor for effective and facile detection of human neutrophil elastase. *Carbohydr. Polym.* **2019**, *216*, 360−368.
(42) Liu, L. G.; Bassett, W. A. Compression of Ag and phase transformation of NaCl. *J. Appl. Phys.* **1973**, *44*, 1475−1479.
(43) Scherrer, P. Bestimmung der Grösse und der inneren Struktur von Kolloidteilchen mittels Röntgenstrahlen. *Nachr. Ges. Wiss. Göttingen* **1918**, *1918*, 98−100.
(44) Langford, J. I.; Wilson, A. J. C. Scherrer after sixty years: A survey and some new results in the determination of crystallite size. *J. Appl. Crystallogr.* **1978**, *11*, 102−113.
(45) Macrae, C. F.; Gruno, I. J.; Chisholm, J. A.; Edginston, P. R.; McCabe, P.; Pidcock, E.; Rodriguez-Monge, L.; Taylor, R.; van de Streek, J.; Wood, P. A. Mercury CSD 2.0-new features for the visualization and investigation of crystal structures. *J. Appl. Crystallogr.* **2008**, *41*, 466−470.
(46) Segal, L.; Creely, J. J.; Martin, A. E.; Conrad, C. M. An empirical method for estimating the degree of crystallinity of native cellulose using X-ray diffractometer. *Text. Res. J.* **1959**, *29*, 786−794.
(47) Wanjura, J. D.; Boman, R. K.; Kelley, M. S.; Ashbrook, C. W.; Faulkner, W. B.; Holt, G. A.; Pelletier, M. G. Evaluation of commercial cotton harvesting systems in the southern high plains. *Appl. Eng. Agric.* **2013**, *29*, 321−332.
(48) Wanjura, J. D.; Baker, K.; Barnes, E. Engineering and ginning: Harvesting. *J. Cotton Sci.* **2017**, *21*, 70−80.
(49) Sluiter, A.; Ruiz, R.; Scarlata, C.; Sluiter, J.; Templeton, D.*Determination of Extractives in Biomass*; National Renewable Energy Laboratory: Denver, CO, 2005; pp 1−12.
(50) Jordan, J. H.; Easson, M. W.; Thompson, S.; Wu, Q. L.; Condon, B. D. Lignin-containing cellulose nanofibers with gradient lignin content obtained from cotton gin motes and cotton gin trash. *Cellulose* **2021**, *28*, 757−773.
(51) Nam, S.; Selling, G. W.; Hillyer, M. B.; Condon, B. D.; Rahman, M. S.; Chang, S. Brown cotton fibers self-produce Ag nanoparticles for regenerating their antimicrobial surfaces. *ACS Appl. Nano Mater.* **2021**, *12*, 13112−13122.
(52) Nam, S.; Baek, I. S.; Hillyer, M. B.; He, Z.; Barnaby, J. Y.; Condon, B. D.; Kim, M. S. Thermosensitive textiles made from silver nanoparticle-filled brown cotton fibers. *Nanoscale Adv.* **2022**, *4*, 3725−3736.
(53) Nam, S.; Hillyer, M. B.; He, Z.; Chang, S.; Edwards, J. V. Self-induced transformation of raw cotton to a nanostructured primary cell wall for a renewable antimicrobial surface. *Nanoscale Adv.* **2022**, *4*, 5404−5416.
(54) Nam, S.; Hinchliffe, D. J.; Hillyer, M. B.; Gary, L.; He, Z. Washable Antimicrobial Wipes Fabricated from a Blend of Nano-composite Raw Cotton Fiber. *Molecules* **2023**, *28*, 1051.
(55) Hu, L.; He, R.; Lu, Z.; Zhang, K.; Bai, X. Step-freeze-drying method for carbon aerogels: a study of the effects on microstructure and mechanical property. *RSC Adv.* **2019**, *9*, 9931−9936.

https://doi.org/10.1021/acsomega.4c05728
ACS Omega 2024, 9, 38195−38204